Transport and thermoelectric properties of n-type Ruddlesden–Popper phase $(Sr_{1-x}Gd_x)_3(Ti_{1-y}Ta_y)_2O_7$ oxides

2012 J. Phys. D: Appl. Phys. 45 415401

(http://iopscience.iop.org/0022-3727/45/41/415401)

J. Phys. D: Appl. Phys. **45** (2012) 415401 (6pp) doi:10.1088/0022-3727/45/41/415401

Transport and thermoelectric properties of n-type Ruddlesden–Popper phase $(Sr_{1-x}Gd_x)_3(Ti_{1-y}Ta_y)_2O_7$ oxides

R R Sun, X Y Qin, L L Li, D Li, J Zhang and Q Q Wang

Key Laboratory of Materials Physics, Institute of Solid State Physics, Chinese Academy of Sciences, 230031 Hefei, People's Republic of China

E-mail: xyqin@issp.ac.cn

Received 6 June 2012, in final form 16 August 2012
Published 28 September 2012
Online at stacks.iop.org/JPhysD/45/415401

Abstract

The transport and thermoelectric properties of $(Sr_{1-x}Gd_x)_3(Ti_{1-y}Ta_y)_2O_7$ ($x = 0.05$, $y = 0.05$–0.15; $x = 0.1$, $y = 0.05$–0.1) compounds with Ruddlesden–Popper (RP) phase, prepared by a conventional solid-state reaction method plus spark plasma sintering (SPS), were investigated in the temperature range from 300 to 1000 K. The results indicate that the electrical resistivity ρ for all compounds increases with temperature, and has a relation $\rho \propto T^M$ (i.e. the mobility $\mu \propto T^{-M}$) with $M = 1.58$–1.92 at $T \gtrsim 650$ K, indicating that the phonon scattering is predominant. Basically, the absolute value of the Seebeck coefficient $|S|$ increases almost linearly with temperature above ~400 K, showing degenerated semiconducting behaviour. Moreover, both ρ and $|S|$ decrease with the increase in both Ta and Gd content, which can be attributed to an increase in the carrier concentration. The lattice thermal conductivity κ_L of the compounds decreases monotonically with an increase in both Ta and Gd content due to mass-defect phonon scattering, and the lowest κ_L ($\kappa_L = 3.3\,W\,K^{-1}m^{-1}$ at room temperature and $2.0\,W\,K^{-1}\,m^{-1}$ at 1000 K) is achieved in $(Sr_{0.9}Gd_{0.1})_3(Ti_{0.9}Ta_{0.1})_2O_7$. Among all the compounds investigated here, the largest dimensionless figure of merit $ZT = 0.08$ (at 1000 K) is obtained in the compound $(Sr_{0.9}Gd_{0.1})_3(Ti_{0.95}Ta_{0.05})_2O_7$.

1. Introduction

Thermoelectric materials, evaluated by a dimensionless figure of merit ($ZT = S^2T/\rho\kappa$, where Z, T, S, ρ and κ are the figure of merit, the absolute temperature, the Seebeck coefficient, the electrical resistivity and the thermal conductivity, respectively), are expected to play an increasingly important role in the application of the conversion between thermal and electrical energy [1–3]. In recent years, metal oxides have been considered to be promising thermoelectric materials at high temperatures due to their non-toxicity and high thermal and chemical stability. The Sr–Ti–O system is one of the best n-type oxide thermoelectric materials ever reported. $SrTiO_3$ is a band insulator, which has an empty conduction band including mainly Ti3d orbitals and a filled valence band containing O2p orbitals [4]. However, low electrical resistivity in $SrTiO_3$ can be achieved through heat treatment in a reducing atmosphere or by doping [4]. It turns out that intensive electron doping is an effective way to reduce the electrical resistivity of $SrTiO_3$. For instance, the cubic perovskite-type 20% Nb-doped $SrTiO_3$ epitaxial film has been found to exhibit the largest ZT (~0.37) at 1000 K [5], and the La-doped single crystal has the largest ZT of 0.27 at 1073 K [6]. However, the ZT values of the oxides are not large enough for practical applications. As a matter of fact, the low performance of the $SrTiO_3$ system can be ascribed to the relatively high thermal conductivity κ ($\kappa = 12\,W\,m^{-1}\,K^{-1}$ at 300 K and $3.1\,W\,m^{-1}\,K^{-1}$ at 1000 K), which is about one order of magnitude larger than that of Bi_2Te_3 alloys [7]. In order to suppress κ, many efforts have been made, such as an isovalent substitution of Eu^{2+}at Sr sites in 20% Nb-doped $SrTiO_3$ epitaxial films [8] and Sr-site substitution with Ca or Ba in Nb-doped $SrTiO_3$ [9], but the results of these studies are disappointing.

In order to reduce κ in the Sr–Ti–O system, attention has been paid to the layered perovskite-type $Sr_{n+1}Ti_nO_{3n+1}$ (n = integer) compounds. These compounds have a superlattice-like structure, which is known as Ruddlesden–Popper (RP)

phase, that is built up with alternate stacks of SrO layers and perovskite $(SrTiO_3)_n$ block layers along the c-axis [10, 11]. In this inherent superlattice-like structure, κ is expected to reduce drastically by the enhancement of phonon scattering at the internal interfaces of $SrO/(SrTiO_3)_n$, and a high power factor PF ($= S^2/\rho$) would be maintained due to the presence of $(SrTiO_3)_n$ block layers, which act as conducting layers. To date, two series of n-type $Sr_{n+1}Ti_nO_{3n+1}$ ($n = 1$ or 2) compounds doped with Nb^{5+}at Ti sites and with rare-earth metals (Gd^{3+}, Sm^{3+}, Nd^{3+} and La^{3+}) at Sr sites have been investigated by Lee *et al* [12, 13] and Wang *et al* [14–17], and their results show that κ of the RP phase oxides decreases by ~60% at room temperature and by ~30% at 1000 K as compared with that of $SrTiO_3$, and the largest $ZT_{1000\,K} \sim 0.24$ was obtained in 5% Gd-doped $Sr_3Ti_2O_7$. Lee *et al* [18] reported that the ZT value of Nb-doped $Sr_3Ti_2O_7$ was improved by an isovalent substitution at Sr sites with Ca^{2+} due to the additional reduction in the lattice thermal conductivity κ_L caused by the mass-defect phonon scattering.

As mentioned above, κ of the Sr–Ti–O system could be reduced substantially in the layered perovskite-type $Sr_{n+1}Ti_nO_{3n+1}$ compounds. However, the ZT value of the RP phase oxides is still very low, and studies on the effect of element doping on their thermoelectric properties are very limited. For instance, there are no studies on the double-doped $Sr_3Ti_2O_7$ compounds using heavy elements with higher valence (doping with trivalent ions at Sr sites and with quinquevalence ions at Ti sites simultaneously), which is expected to reduce the lattice thermal conductivity effectively and increase the carrier concentration as well. Hence, further investigations on the influence of element doping, such as substitutions of heavy elements at Sr or Ti sites and both sites simultaneously, on the transport and thermoelectric properties are imperative, and have great significance in the improvement of this oxide system. In this study, double-doped compounds $(Sr_{1-x}Gd_x)_3(Ti_{1-y}Ta_y)_2O_7$ ($x = 0.05$, $y = 0.05$–0.15; $x = 0.1$, $y = 0.05$–0.1) (doping Gd at Sr sites and Ta at Ti sites simultaneously) were prepared, and their transport and thermoelectric properties including the electrical resistivity ρ, the Seebeck coefficient S and the thermal conductivity κ were investigated in the temperature range from 300 to 1000 K. The obtained results were discussed based on the variations of the thermoelectric parameters with temperature.

2. Experimental procedures

Polycrystalline powder samples of $(Sr_{1-x}Gd_x)_3(Ti_{1-y}Ta_y)_2O_7$ ($x = 0.05$, $y = 0.05$–0.15; $x = 0.1$, $y = 0.05$–0.1) were prepared from $SrCO_3$ (AR), TiO_2 (AR), Gd_2O_3 (99.99%) and Ta_2O_5 (99.99%) by a conventional solid-state reaction method. Appropriate amounts of the starting materials were ball-milled for about 6 h in a planetary ball mill. The ball-milled powders were dried and calcined at 1200 °C twice to decompose the carbonate. In order to form the RP phase and generate the electron carriers, the calcined powders were treated at 1500 °C several times in a mixture of H_2 and Ar gases. And then, the obtained powders were placed in a graphite die of 20 mm in diameter and spark plasma sintered for 5 min at 1525 °C under a pressure of 40 MPa in an Ar flow. Finally, the obtained bulk samples were re-treated at 1500 °C for 2 h in a flow of Ar and H_2 gases to ensure the homogeneity of the bulk samples. X-ray diffraction (XRD) patterns were used to determine the phase structure of all the samples. Accurate lattice parameters a, c and the volume of the unit cell V were calculated using a Si standard for calibration based on the XRD patterns. The electrical resistivity ρ and the Seebeck coefficient Swere measured simultaneously in ZEM-3 (Ulvac Riko, Inc.). The Hall coefficients at room temperature were measured by applying a field of 250 mT, and the carrier concentration n and mobility μ were determined using the measured electrical resistivity and Hall coefficients. The total thermal conductivity κ was calculated from the formula $\kappa = \alpha C_p \lambda$, where α is the thermal diffusivity measured using a laser flash method (Netzsch, LFA 457), C_p is the heat capacity measured by differential scanning calorimetry (DSC, Perkin-Elmer) and λ is the bulk density measured using the Archimedes method, respectively.

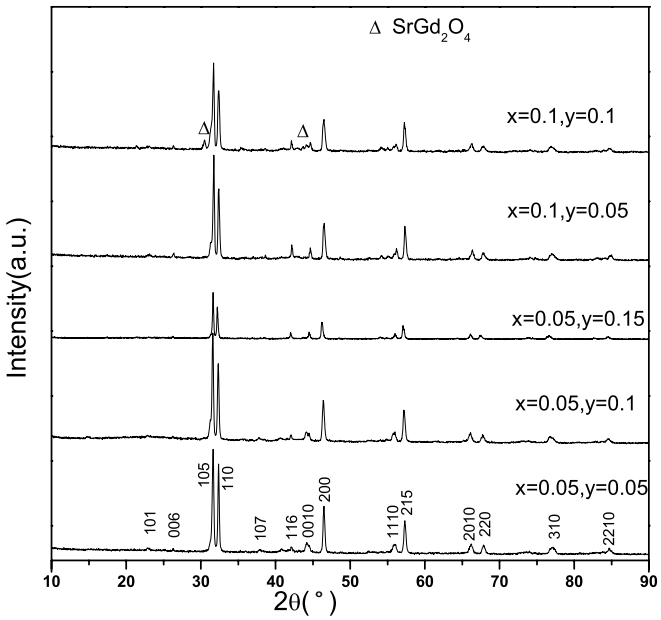

Figure 1. XRD patterns for $(Sr_{1-x}Gd_x)_3(Ti_{1-y}Ta_y)_2O_7$ ($x = 0.05$, $y = 0.05$–0.15; $x = 0.1$, $y = 0.05$–0.1).

3. Results and discussion

3.1. Microstructural characterization

XRD patterns of $(Sr_{1-x}Gd_x)_3(Ti_{1-y}Ta_y)_2O_7$ ($x = 0.05$, $y = 0.05$–0.15; $x = 0.1$, $y = 0.05$–0.1) at room temperature are shown in figure 1. It can be seen that the $Sr_3Ti_2O_7$ single phase was basically formed in the compounds $(Sr_{1-x}Gd_x)_3(Ti_{1-y}Ta_y)_2O_7$ ($x = 0.05$, $y = 0.05$–0.15; $x = 0.1$, $y = 0.05$), while a small amount of $SrGd_2O_4$ phase as a secondary phase was detected in the compound $(Sr_{0.9}Gd_{0.1})_3(Ti_{0.9}Ta_{0.1})_2O_7$. In order to explain this result, we introduce the Goldschmidt tolerance factor t, well known as a basic parameter of perovskite crystals structural distortion, which can be expressed as $t = (r_A + r_O)/\sqrt{2}(r_B + r_O)$, where r_A,

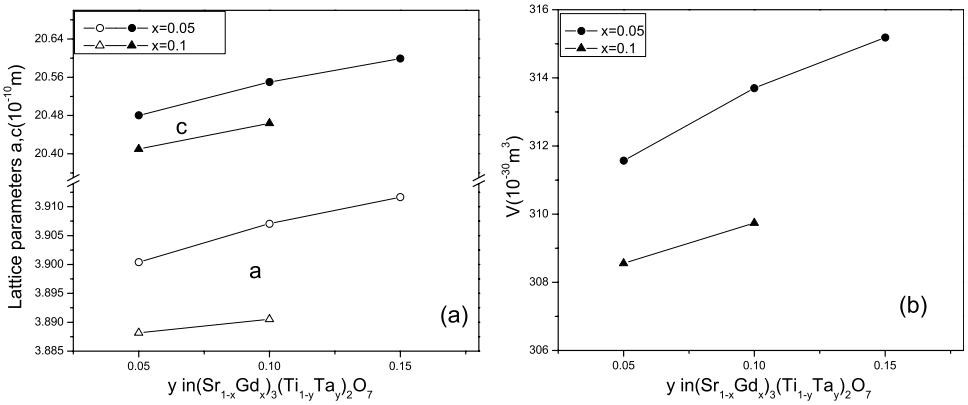

Figure 2. Variations of lattice parameters a, $c(a)$ and the volume of the unit cell V (b) with Ta content for $(Sr_{1-x}Gd_x)_3(Ti_{1-y}Ta_y)_2O_7$ with different Gd content ($x = 0.05$ and 0.1) at room temperature.

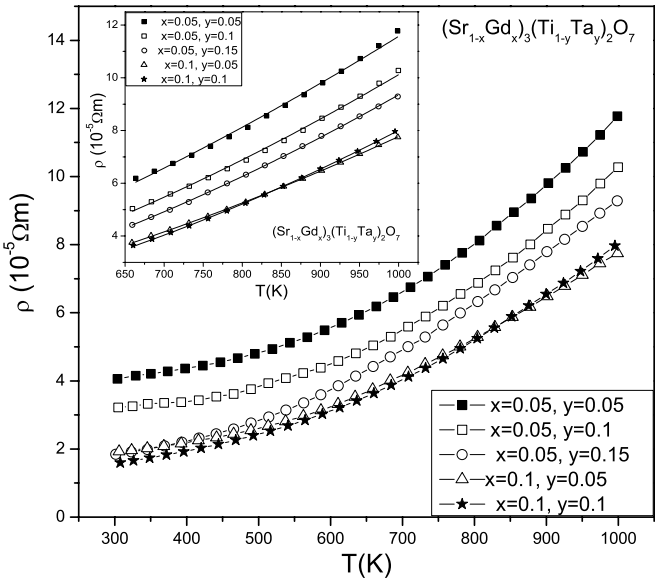

Figure 3. Temperature dependence of the electrical resistivity ρ for $(Sr_{1-x}Gd_x)_3(Ti_{1-y}Ta_y)_2O_7$ ($x = 0.05$, $y = 0.05$–0.15; $x = 0.1$, $y = 0.05$–0.1). The inset shows the magnified plots of ρ versus temperature in the temperature range 650–1000 K, and the solid line in the inset is the fit to formula (1).

r_B and r_O are the average ionic radius of A-site cation, B-site cation and oxygen ion, respectively [19, 20]. The perovskite-type structure will become more stable when the tolerance factor t is close to 1. Since the tolerance factor t would be decreased by doping Ta at Ti sites and Gd at Sr sites, it is easily understood that there exists a solubility limit of Ta at Ti sites and Gd at Sr sites. Thus, when the Ta and Gd doping content increases to a certain value, the structure will become unstable, and a second phase begins to appear.

To check whether the substitutions of Gd for Sr and Ta for Ti have taken place, the accurate lattice parameters a, c and the volume of the unit cell V for all the prepared compounds were calculated based on the XRD patterns (see figures 2(a) and (b)). It can be seen that a, c and V increase gradually with increasing Ta content y, and decrease with an increase in Gd content x. For instance, the lattice parameter a increases from 3.900 to 3.912 Å as y increases from 0.05 to 0.15 for the compounds $(Sr_{1-x}Gd_x)_3(Ti_{1-y}Ta_y)_2O_7$ with $x = 0.05$. All these results indicate that both substitutions of Gd for Sr and Ta for Ti have occurred, for the radius of Ta^{5+} (ionic radius $r_{Ta^{5+}} = 0.64$ Å, coordination number = 6) is slightly larger than that of Ti^{4+} ($r_{Ti^{4+}} = 0.61$ Å, coordination number = 6), which should result in lattice expansion after substitution of Ta for Ti, and Gd^{3+} ($r_{Gd^{3+}} = 1.107$ Å, coordination number = 9) has smaller radius than Sr^{2+} ($r_{Sr^{2+}} = 1.31$ Å, coordination number = 9), thus leading to lattice contraction [21, 22].

Table 1. List of parameters ρ_0 and M for $(Sr_{1-x}Gd_x)_3(Ti_{1-y}Ta_y)_2O_7$ ($x = 0.05$, $y = 0.05$–0.15; $x = 0.1$, $y = 0.05$–0.1).

$(Sr_{1-x}Gd_x)_3(Ti_{1-y}Ta_y)_2O_7$	ρ_0 ($10^{-10}\,\Omega\,m\,K^{-M}$)	M
$x = 0.05$, $y = 0.05$	20.60	1.58
$x = 0.05$, $y = 0.1$	6.92	1.72
$x = 0.05$, $y = 0.15$	3.71	1.80
$x = 0.1$, $y = 0.05$	4.27	1.75
$x = 0.1$, $y = 0.1$	1.38	1.92

3.2. Transport and thermoelectric properties

3.2.1. Electrical resistivity ρ and Seebeck coefficient S. Plots of the electrical resistivity ρ versus temperature for $(Sr_{1-x}Gd_x)_3(Ti_{1-y}Ta_y)_2O_7$ ($x = 0.05$, $y = 0.05$–0.15; $x = 0.1$, $y = 0.05$–0.1) in the investigated temperature range are presented in figure 3. We can see that the variation of ρ for all compounds is similar: ρ increases gradually with increasing temperature, showing metallic-like behaviour. Above ~650 K, the electrical resistivity ρ in all cases obeys a power law, i.e. it can be expressed as

$$\rho = \rho_0 T^M. \tag{1}$$

By best fitting the experimental data to formula (1), one obtains the parameters ρ_0 and M, which are listed in table 1. It can be seen from table 1 that ρ_0 decreases with both Gd and Ta content, whereas M increases. For instance, ρ_0 decreases from 2.06×10^{-9} to $3.71 \times 10^{-10}\,\Omega\,mK^{-M}$, and M increases from 1.58 to 1.80 for $(Sr_{1-x}Gd_x)_3(Ti_{1-y}Ta_y)_2O_7$ with $x = 0.05$ when the Ta content y increases from 0.05 to 0.15. It is convenient to express the electrical resistivity as $\rho = 1/ne\mu$, where n, e and μ are the carrier concentration,

Table 2. List of carrier concentration n, the electrical resistivity ρ, Hall mobility μ and carrier effective mass $m*$ for $(Sr_{1-x}Gd_x)_3(Ti_{1-y}Ta_y)_2O_7$ ($x = 0.05$, $y = 0.05$–0.15; $x = 0.1$, $y = 0.05$–0.1) at room temperature.

$(Sr_{1-x}Gd_x)_3(Ti_{1-y}Ta_y)_2O_7$	$n(10^{21}\,cm^{-3})$	$\rho(10^{-5}\,\Omega\,m)$	$\mu(cm^2\,V^{-1}\,s^{-1})$	m^* (m_0)
$x = 0.05,\quad y = 0.05$	0.9	4.06	1.7	1.7
$x = 0.05,\quad y = 0.1$	1.2	3.22	1.6	1.4
$x = 0.05,\quad y = 0.15$	1.9	1.84	1.8	1.1
$x = 0.1,\quad y = 0.05$	1.5	1.92	2.2	1.5
$x = 0.1,\quad y = 0.1$	2.3	1.60	1.7	1.6

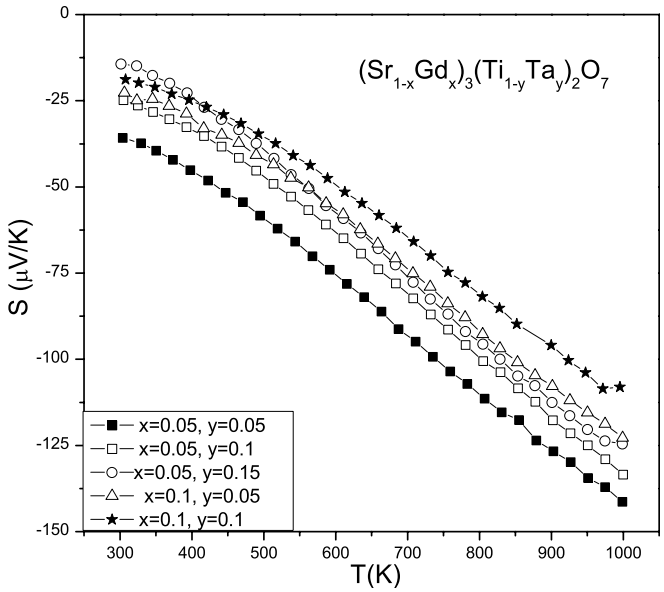

Figure 4. Temperature dependence of the Seebeck coefficient S for $(Sr_{1-x}Gd_x)_3(Ti_{1-y}Ta_y)_2O_7$ ($x = 0.05$, $y = 0.05$–0.15; $x = 0.1$, $y = 0.05$–0.1).

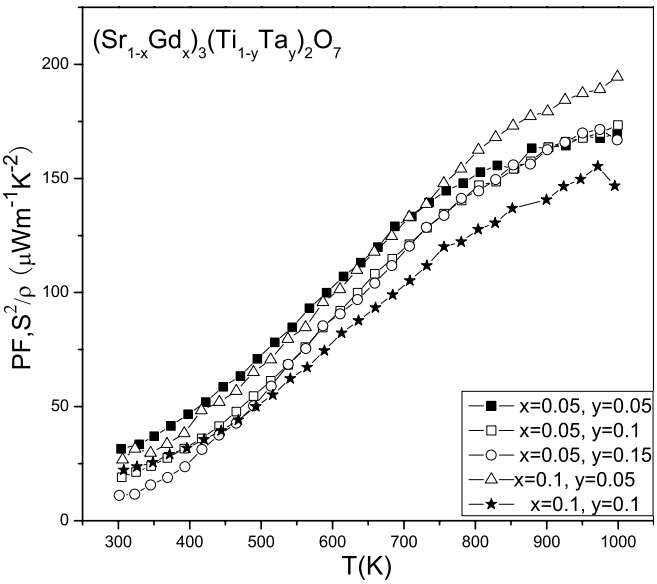

Figure 5. Plots of power factor (PF) versus temperature for $(Sr_{1-x}Gd_x)_3(Ti_{1-y}Ta_y)_2O_7$ ($x = 0.05$, $y = 0.05$–0.15; $x = 0.1$, $y = 0.05$–0.1).

the electron charge and the mobility, respectively. For a given nominal composition, the carrier concentration does not change remarkably in a certain high-temperature range, as verified by some researchers [5, 14, 18]. We can, therefore, obtain the relation of mobility μ with parameter M, i.e. $\mu \propto T^{-M}$ ($1.58 \leqslant M \leqslant 1.92$), which indicates that the acoustic phonon scattering mechanism is predominant [23]. Moreover, the electrical resistivity ρ basically decreases with the increase in both Ta and Gd content. For instance, ρ at room temperature decreases from 4.06 to 1.84 mΩ cm for $(Sr_{1-x}Gd_x)_3(Ti_{1-y}Ta_y)_2O_7$ with $x = 0.05$ as y increases from 0.05 to 0.15. Since the doped Gd atoms and Ta atoms are expected to act as donors, electron carrier concentration should increase with increasing doping content of Gd and/or Ta, which is confirmed by our direct measurements of carrier concentration, as given in table 2.

Figure 4 shows the temperature dependence of the Seebeck coefficient S for $(Sr_{1-x}Gd_x)_3(Ti_{1-y}Ta_y)_2O_7$ ($x = 0.05$, $y = 0.05$–0.15; $x = 0.1$, $y = 0.05$–0.1) in the temperature range from 300 to 1000 K. All the samples have a negative Seebeck coefficient S, indicating that the major charge carriers are electrons. Above ∼400 K, the absolute value of the Seebeck coefficient $|S|$ in all cases increases almost linearly with temperature, implying that all the compounds are in degenerate states. This suggests that in the high-temperature range (400 K $< T <$ 1000 K) the Seebeck coefficient of the doped compounds can be expressed as [24] (Mott formula):

$$S = \frac{\pi^2 K_B^2 T}{3e}\left[\frac{\partial \ln \sigma(E)}{\partial E}\right]_{E_f} = \frac{C_e(T)}{ne} + \frac{\pi^2 K_B^2 T}{3e}\left[\frac{\partial \ln \mu(E)}{\partial E}\right]_{E_f} \quad (2)$$

with

$$C_e = \frac{\pi^2 K_B^2 T}{3e} g(\varepsilon), \quad (3)$$

where C_e is the electronic heat capacity, $g(\varepsilon)$ is the density of states, $\sigma = 1/\rho$ is the electrical conductivity, K_B is the Boltzmann constant and E_f is the Fermi level. However, it should be noted here that there exists obvious deviation from linear relationship as $T \lesssim 400$ K. This suggests that a transition from degenerate state to non-degenerate state occurs when the temperature is below 400 K, where relation (2) could not hold. Moreover, one can see that $|S|$ decreases monotonically with the increase in both Gd and Ta content in the entire temperature range studied here. For instance, $|S|$ at 300 K decreases from 36 μV K^{-1} for $x = 0.05$ to 23 μV K^{-1} for $x = 0.1$ when the Ta content y is fixed at 0.05. This may be attributed to the increase in carrier concentration with increasing of both Gd and Ta content, as shown in table 2. Since the carrier effective mass m^* is one of the most important factors determining S,

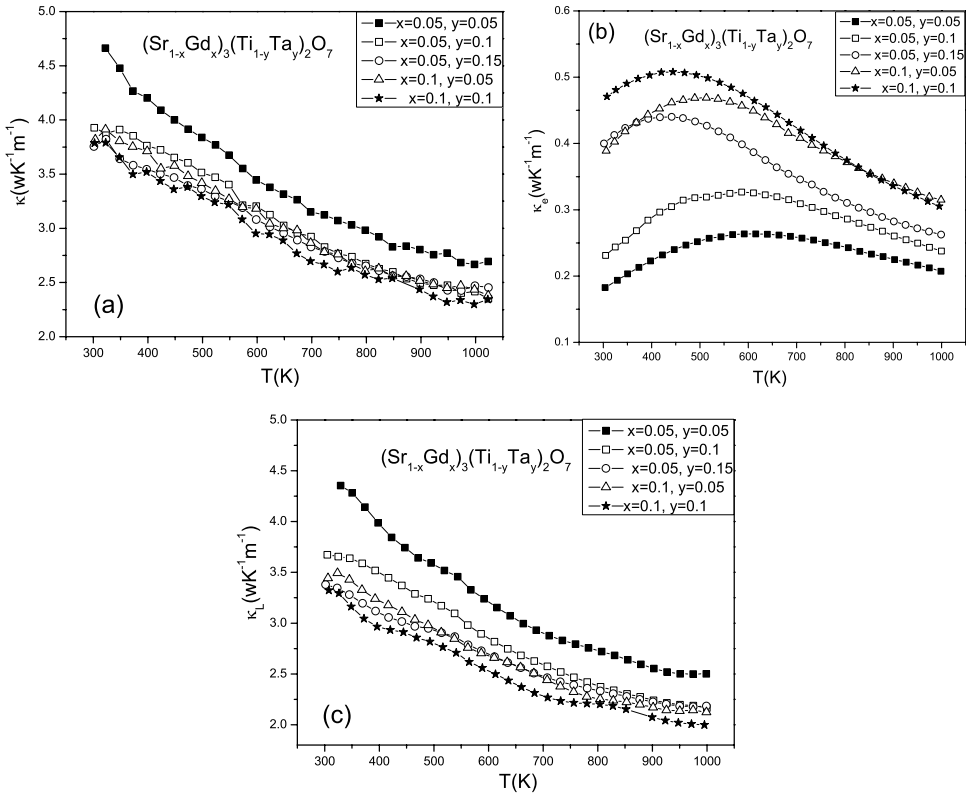

Figure 6. Variations of the total thermal conductivity κ (*a*), electronic thermal conductivity κ_e (*b*) and lattice thermal conductivity κ_L (*c*) with temperature for $(Sr_{1-x}Gd_x)_3(Ti_{1-y}Ta_y)_2O_7$ ($x = 0.05$, $y = 0.15$–0.15; $x = 0.1$, $y = 0.05$–0.1).

the m^* values at room temperature for the compounds with different doping contents were calculated (assuming that the acoustic phonon scattering is predominant here) using the method described elsewhere [6, 12, 25]. As shown in table 2, the values of the obtained m^* range from 1.1 to 1.7 m_0 (here m_0 is the free electron mass), which does not change remarkably with both Gd and Ta content. The current results are basically in agreement with previous reports [18].

Plots of the power factor (PF $= S^2/\rho$) versus temperature for $(Sr_{1-x}Gd_x)_3(Ti_{1-y}Ta_y)_2O_7$ ($x = 0.05$, $y = 0.05$–0.15; $x = 0.1$, $y = 0.05$–0.1), calculated from S and ρ, are shown in figure 5. It can be easily seen that the temperature dependence of PF for all compounds is similar, increasing consistently with temperature. Among all the compounds we investigated, $(Sr_{0.9}Gd_{0.1})_3(Ti_{0.95}Ta_{0.05})_2O_7$ has the largest PF (195 μW m^{-1} K^{-2}) at 1000 K.

3.2.2. Thermal conductivity κ and the dimensionless figure of merit ZT. Figure 6(*a*) shows the total thermal conductivity κ for $(Sr_{1-x}Gd_x)_3(Ti_{1-y}Ta_y)_2O_7$ ($x = 0.05$, $y = 0.05$–0.15; $x = 0.1$, $y = 0.05$–0.1) as a function of temperature. One can see that κ for all the doped compounds decreases monotonically with increasing temperature. Apart from the compound $(Sr_{0.95}Gd_{0.05})_3(Ti_{0.95}Ta_{0.05})_2O_7$, the differences in κ for the other compounds are relatively small. The total thermal conductivity κ includes the lattice thermal conductivity κ_L and the electronic contribution κ_e. The κ_e values can be calculated using the Wiedemann–Franz law expressed by

$$\kappa_e = L_0 T/\rho, \tag{4}$$

where L_0 is the Lorentz number (here $L_0 = 2.443 \times 10^{-8}$ W Ω K^{-2} for free electron is adopted for the estimation). The temperature dependences of κ_e and κ_L for $(Sr_{1-x}Gd_x)_3(Ti_{1-y}Ta_y)_2O_7$ ($x = 0.05$, $y = 0.05$–0.15; $x = 0.1$, $y = 0.05$–0.1) are shown in figures 6(*b*) and (*c*), respectively. The κ_e value basically increases with increasing Ta and Gd content due to the increased carrier contribution. However, all the samples have very small κ_e (<0.5 W K^{-1} m^{-1}), indicating that the phonon contribution is predominant. Moreover, one can see from figure 6(*c*) that the lattice thermal conductivity κ_L (specially at $T < 700$ K) decreases obviously with the increase in both Ta and Gd content due to enhanced phonon scattering by the impurities (dopants). For instance, as $x = 0.05$ κ_L at room temperature decreases from 4.4 W m^{-1} K^{-1} for $y = 0.05$ to 3.7 W m^{-1} K^{-1} for $y = 0.1$, and then to 3.4 W m^{-1} K^{-1} for $y = 0.15$. Likewise, κ_L decreases with increasing Gd content x at a given y. However, it is worthwhile to note that both κ and κ_L of the compound $(Sr_{0.95}Gd_{0.05})_3(Ti_{0.95}Ta_{0.05})_2O_7$ are obviously larger than those of the other compounds, and the thermal conductivity differences among the other heavily doped compounds are relatively small. The reason for this phenomenon may lie in the following factors: (1) among all the compounds, $(Sr_{0.95}Gd_{0.05})_3(Ti_{0.95}Ta_{0.05})_2O_7$ contains the lowest content of dopants, which would produce weakest phonon scattering; (2) as dopant content (x or/and y) increases, phonon scattering enhances, leading to a large decease in thermal conductivity (κ and κ_L); (3) as the dopant content (x or/and y) increases further, the phonon scattering effect becomes weak, and the decrease

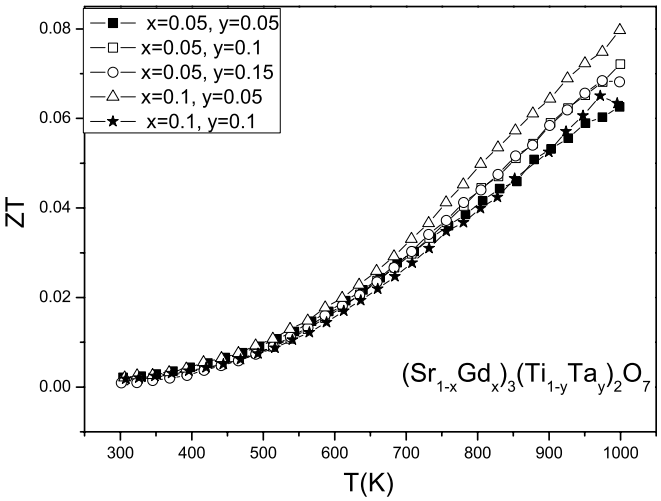

Figure 7. Temperature dependence of the dimensionless figure of merit *ZT* for $(Sr_{1-x}Gd_x)_3(Ti_{1-y}Ta_y)_2O_7$ ($x = 0.05$, $y = 0.05$–0.15; $x = 0.1$, $y = 0.05$–0.1).

in thermal conductivity (κ and κ_L) slows down at high impurity contents, making the thermal conductivity differences among the other heavily doped samples small. Among all the investigated compounds, $(Sr_{0.9}Gd_{0.1})_3(Ti_{0.9}Ta_{0.1})_2O_7$ exhibits the lowest κ_L ($\kappa_L = 3.3\,W\,K^{-1}\,m^{-1}$ at room temperature and $2.0\,W\,K^{-1}\,m^{-1}$ at 1000 K) due to the highest dopant content. The drop in κ_L after doping could be attributed to the mass-defect phonon scattering between Ta (Gd) ($M_{Ta} = 180.9$, $M_{Gd} = 157.3$) and Ti (Sr) ($M_{Ti} = 47.9$, $M_{Sr} = 87.6$) [18].

Based on the values of S, ρ and κ, the dimensionless figure of merit ZT for $(Sr_{1-x}Gd_x)_3(Ti_{1-y}Ta_y)_2O_7$ ($x = 0.05$, $y = 0.05$–0.15; $x = 0.1$, $y = 0.05$–0.1) was calculated, as shown in figure 7. The ZT value for all samples increases monotonically with increasing temperature. Obviously, there is no obvious difference in ZT values among the compounds doped with both different elements and their contents at temperatures below 600 K. Among all the compounds investigated here, the largest ZT is 0.08 achieved in $(Sr_{0.9}Gd_{0.1})_3(Ti_{0.95}Ta_{0.05})_2O_7$ at 1000 K.

4. Summary

RP phase compounds of $(Sr_{1-x}Gd_x)_3(Ti_{1-y}Ta_y)_2O_7$ ($x = 0.05$, $y = 0.05$–0.15; $x = 0.1$, $y = 0.05$–0.1) were prepared, and their transport and thermoelectric properties were measured in the temperature range from 300 to 1000 K. The results indicate that both the resistivity ρ and the absolute value of the Seebeck coefficient $|S|$ (here $S < 0$) increase with temperature for all the doped compounds, and decrease with the increase in both Ta and Gd content due to the increase in carrier concentration. Above ~650 K, the electrical resistivity obeys a power law $\rho = \rho_0 T^M$ with their exponent M varying from 1.58 for $x = 0.05$ and $y = 0.05$ to 1.92 for $x = 0.1$ and $y = 0.1$. The small contribution of κ_e ($<0.5\,W\,K^{-1}\,m^{-1}$) for all samples indicates that the phonon contribution is predominant. The lattice thermal conductivity κ_L decreases with both Ta and Gd content which can be ascribed to the mass-defect phonon scattering, and the lowest κ_L ($\kappa_L = 3.3\,W\,K^{-1}\,m^{-1}$ at room temperature and $2.0\,W\,K^{-1}\,m^{-1}$ at 1000 K) is achieved in $(Sr_{0.9}Gd_{0.1})_3(Ti_{0.9}Ta_{0.1})_2O_7$. ZT for all compounds increases monotonically with temperature. Among all the compounds we investigated, $(Sr_{0.9}Gd_{0.1})_3(Ti_{0.95}Ta_{0.05})_2O_7$ exhibits the largest $ZT = 0.08$ at 1000 K.

Acknowledgment

Financial support from the National Natural Science Foundation of China (Nos 50972146, 10904144, 11174292 and 51101150) is gratefully acknowledged.

References

[1] Rowe D M (ed) 1995 *CRC Handbook of Thermoelectrics* (Boca Raton, FL: CRC Press)
[2] Disalvo F J 1999 *Science* **285** 703
[3] Snyder G J and Toberer E S 2008 *Nature. Mater.* **7** 105–14
[4] Ohtaki M 2010 Oxide Thermoelectric materials for heat-to-electricity direct energy conversion *Kyushu University Global COE Program Novel Carbon Resources Sciences Newsletter* vol 3 (Special issue)
[5] Ohta S, Nomura T, Ohta H, Hirano M, Hosono H and Koumoto K 2005 *Appl. Phys. Lett.* **87** 092108
[6] Ohta S, Nomura T, Ohta H and Koumoto K 2005 *J. Appl. Phys.* **97** 034106
[7] Ohta S, Ohta H and Koumoto K 2006 *J. Ceram. Soc. Japan.* **114** 102–5
[8] Kato K, Yamamoto M, Ohta S, Muta H, Kurosaki K, Yamanaka S, Iwasaki H, Ohta H and Koumoto K 2007 *J. Appl. Phys.* **102** 116107
[9] Yamamoto M, Ohta H and Koumoto K 2007 *Appl. Phys. Lett.* **90** 072101
[10] Ruddlesden S N and Popper P 1957 *Acta Crystallogr.* **10** 538–9
[11] Ruddlesden S N and Popper P 1958 *Acta Crystallogr.* **11** 54–55
[12] Lee K H, Ohta H, Kim S W and Koumoto K 2006 *J. Appl. Phys.* **100** 063717
[13] Lee K H, Wang Y F, Kim S W, Ohta H and Koumoto K 2007 *Int. J. Ceram. Technol.* **4** 326–31
[14] Wang Y F, Lee K H, Hyuga H, Kita H, Ohta H and Koumoto K 2010 *J. Electroceram.* **24** 76–82
[15] Wang Y F, Lee K H, Ohta H and Koumoto K 2008 *Ceram. Int.* **34** 849–52
[16] Wang Y F, Lee K H, Ohta H and Koumoto K 2009 *J. Appl. Phys.* **105** 103701
[17] Wang Y F, Lee K H, Hyuga H, Kita H, Inaba K, Ohta H and Koumoto K 2007 *Appl. Phys. Lett.* **91** 242102
[18] Lee K H, Kim S W, Ohta H and Koumoto K 2007 *J. Appl. Phys.* **101** 083707
[19] Johnsson M and Lemmens P 2006 Crystallography and chemistry of perovskites *Handbook of Magnetism and Advanced Magnetic Media* ed H Kronmüller (New York: Wiley)
[20] Goldschmidt V M 1926 *Akad. Oslo I. Mat.-Nature* **2** 7
[21] Shannon R D 1976 *Acta Crystallogr.* A **32** 751–67
[22] Jia Y Q 1991 *J. Solid State Chem.* **95** 184–7
[23] Moos R, Schöllhammer S and Härdtl K H 1997 *Appl. Phys.* A **65** 291–4
[24] Blatt F J, Schroeder P A, Foiles C L and Greig D 1976 *Thermoelectric Power of Metals* (New York: Plenum)
[25] Fistul V I 1969 *Heavily Doped Semiconductors* (New York: Plenum)